





## Karavannoe: Mineralogy, trace element geochemistry, and origin of Eagle Station group pallasites

Svetlana N. TEPLYAKOVA <sup>\*</sup>1, Cyril A. LORENZ <sup>1</sup>, Marina A. IVANOVA <sup>1</sup>,  
Munir HUMAYUN <sup>2</sup>, Nataliya N. KONONKOVA<sup>1</sup>, Sergey E. BORISOVSKY<sup>3</sup>,  
Alexander V. KOROCHANTSEV<sup>1</sup>, Ian A. FRANCHI <sup>4</sup>, and Nina G. ZINOVIEVA<sup>5</sup>

<sup>1</sup>Vernadsky Institute of Geochemistry and Analytical Chemistry, Moscow 119991, Russia

<sup>2</sup>National High Magnetic Field Laboratory and Department of Earth, Ocean & Atmospheric Science, Florida State University, 1800 E. Paul Dirac Drive, Tallahassee, Florida 32310, USA

<sup>3</sup>Institute of Geology of Ore Deposits, Petrography, Mineralogy, and Geochemistry RAS, Staromonetnyi per, 35, Moscow 119017, Russia

<sup>4</sup>Planetary and Space Sciences Research Institute, Open University, Milton Keynes MK7 6AA, UK

<sup>5</sup>Lomonosov Moscow State University, GSP-1, Leninskie Gory, Moscow 119991, Russia

\*Corresponding author. E-mail: elga.meteorite@gmail.com

(Received 26 February 2021; revision accepted 18 March 2022)

---

**ABSTRACT**—Karavannoe is a pallasite found in Russia in 2010. The mineralogy, chemistry, and oxygen isotopic composition indicate that Karavannoe is a member of the Eagle Station Pallasite (ESP) group. Karavannoe contains mostly olivine and subdued interstitial Fe,Ni-metal. Zoned distribution of FeO in small, rounded grains of olivine and FeO and Al<sub>2</sub>O<sub>3</sub> in chromite shows that the cooling rate of the melt was fast during the crystallization of the round olivine grains. Siderophile element distribution and correlations of Au-As and Os-Ir concentrations in Karavannoe and the other ESP metal record its magmatic origin. FeO-rich composition of olivine, low W and Ga, and high Ni abundances in the Karavannoe metal indicate the formation of the metal from an oxidized chondrite precursor. Model calculations demonstrate that the ESPs' metal compositions correspond to the solids of the fractional crystallization of CV- or CO-chondrite-derived metallic liquids. The Karavannoe metal composition corresponds to the solid fraction crystallized after ~40% fractional crystallization. The Mg/(Mg+Fe) atom ratio of complementary silicate liquid corresponds to Fo<sub>70</sub>, possibly indicating that the olivine is not in equilibrium with the metal and could have been a product of the late evolutionary processes in the Karavannoe parent body mantle. In any ESP genesis Karavannoe was not in equilibrium with its metal and is a product of mantle differentiation processes. Olivine of Karavannoe and ESPs is similar in composition, while the metal is different. We propose a model of ESP formation involving an impact-induced intrusion of liquid core metal into a basal mantle layer, followed by fractional crystallization of the metal. The metal textures and chemical zoning of Karavannoe minerals point to remelting and rapid cooling due to a later impact event.

---

### INTRODUCTION

Among all types of differentiated meteorites, 141 pallasites are known (Meteoritical Bulletin Database; <https://www.lpi.usra.edu/meteor/>). Based on oxygen isotope composition, trace element concentrations in the Fe,Ni-metal, and mineralogical composition, the pallasites are subdivided into several groups that

originated from separate parent bodies: the main group (MG) pallasites; the Eagle Station pallasites (ESPs); the pyroxine pallasites (Vermillion, Yamato 8451); and several ungrouped pallasites including Choteau, Milton, Zinder, Northwest Africa 1911, and Northwest Africa 10019 (Agee et al., 2015; Boesenberg et al., 2012; Gregory et al., 2016; McCoy et al., 2019; Scott, 2007; Yang et al., 2010). The primary hypothesis of MG pallasite origin is

that they were formed at the core–mantle boundary of their parent body (Rayleigh, 1942; Scott, 1977a, 1977b, 1977c, 2007; Scott & Taylor, 1990; Ulf-Müller, 1998; Wasson & Choi, 2003; Yang et al., 2010). Other authors (Carpörzen et al., 2011; Elkins-Tanton et al., 2011; Hsu, 2003; Tarduno et al., 2014) consider that pallasites have not necessarily formed at the core–mantle boundary of their parent bodies, and based on pallasite thermal histories, they may have formed at a shallow depth and were subsequently buried deep under a regolith blanket. These models of pallasite genesis alternative to the primary hypothesis of MG pallasite origin imply the formation of pallasites by impact melting and mixing of two separated differentiated parent bodies (Carpörzen et al., 2011; Elkins-Tanton et al., 2011; Tarduno et al., 2014) or through a double impact on the surface of a single parent body (Malvin et al., 1985). Pallasites have also been proposed to be the products of ferrovolcanism, where metallic liquid is intrusive into mantle or even extrusive on the asteroid surface (Abrahams & Nimmo, 2019; Johnson et al., 2020).

The ESP group includes only five members (Cold Bay, Eagle Station, Itzawisis, Karavannoe, and Oued Bourdim 001), which are distinct from the MG pallasites by low  $\Delta^{17}\text{O}$  (Clayton & Mayeda, 1996), more ferrous olivine ( $\text{Fe}_{20}$ ), and higher Ge/Ga ratios and Ni, Co, and Ir contents in their metal (Scott, 1977a; Wasson & Choi, 2003).

It was suggested that the ESP group and IIF irons have affinities in metal geochemistry and oxygen isotopic composition of silicates, and that they may be derived from chemically similar parent bodies during impacts and generation of magma with rapid cooling or large-scale internal melting of the parent body (Hilton et al., 2020; Kracher et al., 1980; Malvin et al., 1985). Hilton et al. (2020) showed recently that ESP metals formed mainly as equilibrium solids from a common liquid and that the ESPs most likely formed by the injection of olivine present at the core–mantle boundary into a metallic core liquid as a result of impact followed by inward crystallization of the core material trapped by the olivine. A possible origin of ESP meteorites from a CV-like chondrite source based on oxygen isotopic composition of silicates and siderophile element geochemistry has been shown by Carpörzen et al. (2011), Elkins-Tanton et al. (2011), Humayun and Weiss (2011), and Humayun et al. (2014). This model implies that achondrites and iron meteorites that originated from the CV chondrite parent asteroid should exist. Paleomagnetic studies have revealed the presence of ancient magnetic fields on the parent bodies of CV carbonaceous chondrites (CCs; Carpörzen et al., 2011) and the ESP group (Tarduno et al., 2014). These could originate from core dynamos operating on partially differentiated chondritic

bodies (Carpörzen et al., 2011) and could be evidence of a differentiated CV-like body. The  $^{26}\text{Al}$ – $^{26}\text{Mg}$  and  $^{128}\text{Hf}$ – $^{128}\text{W}$  chronology data indicate that the ESP parent body was differentiated in the first 4 Myr after calcium–aluminum-rich inclusion formation (Luu et al., 2014).

The Karavannoe pallasite (Humayun et al., 2014; Korochantsev et al., 2013) provides an opportunity for understanding of siderophile element behavior of this rare group as it extends the range of compatible elements noted for the ESP group. In this paper, we combined petrographical, mineralogical, and geochemical data together with a model calculation of fractional crystallization of metallic liquid produced from CV- and CO-like chondritic sources to reconstruct the ESP formation process.

## ANALYTICAL METHODS AND SAMPLES

A massive brown stone has been reported to be located in the roadway of the Karavannoe village since the 1960s (Tuzhinsky region, Kirovsky district, Russia). On September 28, 2010, S. and A. Blednykh recognized its potential significance and sent a sawn specimen to the Vernadsky Institute for detailed investigation, where the sample was identified as a meteorite. No reliable data on the meteorite fall or prerecognition history exist. It appears likely that the sample was moved several times after its excavation, so the location in which it was recognized may not correspond to the place of the first find or fall.

The Karavannoe meteorite is a single specimen of irregular shape, 40–50 cm in diameter, weighing 132 kg (Fig. 1). The meteorite surface is highly corroded; in some areas caverns and a slag-like layer of weathering products are present. A fusion crust has not been preserved.

From the Meteorite Collection of the Russian Academy of Sciences, we received five sawn cut pieces (~20 mm × 10 mm in size each) of Karavannoe with the lowest weathering features available, sampled from a large cut plate, at ~10–15 cm below the meteorite surface, mounted in epoxy and polished. The samples of Karavannoe were preliminarily examined using a Leica DMRX optical microscope (reflected light) equipped with a Leica DFC 320 digital camera at the Laboratory of Meteoritics of the Vernadsky Institute. Back-scattered electron (BSE) images were obtained using SEM TESCAN MIRA 3 at the Laboratory of Meteoritics of the Vernadsky Institute; high voltage was 20 kV, beam current 14 nA.

Chemical compositions of silicates and oxides were analyzed by the electron probe microanalysis method (EPMA) using the JEOL Superprobe JXA-8230 at the Laboratory of High Spatial Resolution Analytical Techniques at the Geological Faculty of Moscow State



Fig. 1. Individual sample of the Karavannoe meteorite. (Color figure can be viewed at [wileyonlinelibrary.com](http://wileyonlinelibrary.com).)

University and the JEOL microprobe JXA-8200 (Institute of Geology of Ore Deposits, Petrography, Mineralogy and Geochemistry of Russian Academy of Sciences) with an accelerating voltage of 20 kV, beam current of 20 nA, and beam size of 1  $\mu\text{m}$ . ZAF correction was applied to introduce corrections for mean atomic number, absorption, and secondary fluorescence.

A set of well-characterized standards was used for EPMA: olivine USNM 111312/444 (Si, Mg, Fe) for olivine; diopside USNM 117733 (Si, Mg, Ca), hypersthene USNM 746 (Fe), microcline USNM 143966 (K) and NaCl (Na, Cl) for pyroxene; chromite NMNH 117075 (Cr, Al, Fe) for chromite; and phosphate NMNH 104021 (P, Ca) for phosphates. The counting time of impulses at the peak for major elements was 30 and 15 s to provide a detection limit of 0.02 wt%.

Stoichiometric synthetic and natural substances were used as standards for measuring minor elements in silicates:  $\text{MnTiO}_3$  for analyses of Ti and Mn;  $\text{Cr}_2\text{O}_3$  for Cr; metallic V for V. The counting time for measuring the peak intensity and background during the analysis was chosen depending on the concentration of the element in order to provide a detection limit of the element of 0.01 wt% (60s for Ti and V; 40s for Mn and Cr).

Chemical compositions of metal and sulfide phases were obtained by EPMA with the Cameca SX 100

microprobe at the Vernadsky Institute using an accelerating voltage of 20 kV, beam current of 20–30 nA, and a beam size of 1  $\mu\text{m}$ . The PAP correction procedure was applied. As standards, we used troilite of Sikhote-Alin for troilite, meteorite Fe,Ni-iron and synthetic Co for metal phases, and meteorite schreibersite for phosphides. The detection limits of the analyzed elements were 0.02 wt%.

Siderophile elements were determined by the laser ablation inductively coupled plasma mass spectrometry (LA-ICP-MS) rastering method in three olivine-free metallic areas,  $\sim 3\text{--}4\text{ mm}^2$  each. Laser ablation ICP-MS analyses were performed with a New Wave UP193FX excimer laser system coupled to a Thermo Element XR at the Plasma Analytical Facility, Florida State University. A 100  $\mu\text{m}$  beam spot scanned at  $10\text{--}25\text{ }\mu\text{m s}^{-1}$ , 50 Hz repetition rate,  $2\text{ GW cm}^{-2}$  fluence was used. Other aspects of the measurement are identical to those previously described (Campbell & Humayun, 1999). Four spots on the metal were analyzed and the results were compared with instrumental neutron activation analysis (INAA) data obtained by G. Wasson (see Table 3) for verification of representativeness of average bulk metal composition of Karavannoe according to the analytical procedure by Wasson and Choi (2003).

A separate split of silicate material of the meteorite, weighing  $\sim 50\text{ mg}$ , was used to measure bulk oxygen isotopic compositions at the Open University (Milton Keynes, UK). The sample was crushed in an agate mortar and pestle. Oxygen isotopic compositions were determined in replicate on  $\sim 2\text{ mg}$  aliquots of the partly homogenized sample by laser fluorination. The samples were heated with a  $\text{CO}_2$  laser (10.6  $\mu\text{m}$ ) in the presence of excess  $\text{BrF}_5$ , and the resulting gas was purified over hot KBr and cryogenic traps and then analyzed on a PRISM III mass spectrometer (VG Isogas Ltd). Analytical precision is  $\sim \pm 0.04\text{‰}$  and  $\pm 0.08\text{‰}$  ( $2\sigma$ ) for  $\delta^{17}\text{O}$  and  $\delta^{18}\text{O}$ , respectively, providing a precision of  $\sim \pm 0.02\text{‰}$  ( $2\sigma$ ) for  $\Delta^{17}\text{O}$ . Details of the procedure are described by Miller et al. (1989).

## RESULTS

### Petrography and Mineral Chemistry

The Karavannoe meteorite comprises coarse-grained greenish-yellow olivine grains enclosed in a Fe,Ni-metal network in a typical pallasite texture (Fig. 2). Modal silicate content is in the range of  $\sim 60\text{ vol\%}$ ; olivine is the dominant mineral; and the modal content of metal, phosphide, phosphate, chromite, and sulfide is  $\sim 40\text{ vol\%}$ . Beside olivine and metal, other minerals' modal content is less than 1 vol%.

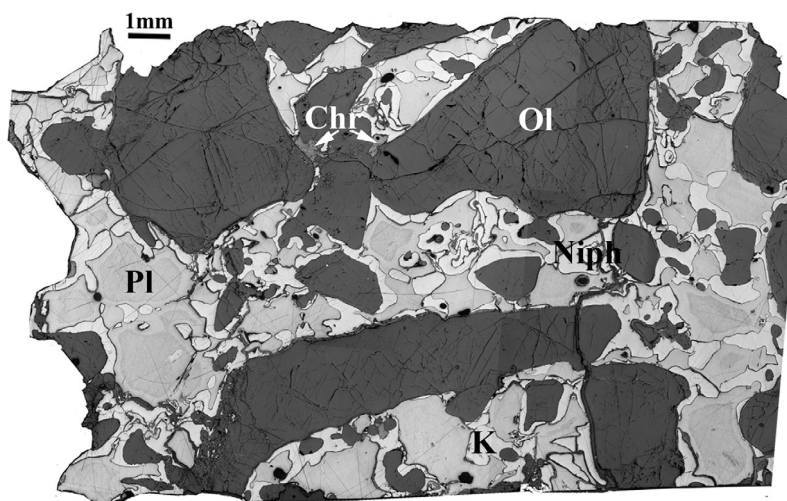


Fig. 2. Microscopic overview of the Karavannoe meteorite in polished and etched section (reflected light). Ol = olivine; K = kamacite; Niph = nickel phosphide; Pl = plessite; Chr = chromite.

The Fe,Ni-metal has a polycrystalline structure and consists of irregular grains of taenite up to 2–3 mm in size (Fig. 2). Subsolidus growth of isometric grains of low-Ni metal phase (“kamacite”) and nickel phosphide (Ni>Fe) along the boundaries of the parent taenite grains and formation of swathing kamacite (Buchwald, 1975) rims along the olivine grain borders, 0.05–0.5 width mm in size, around olivine and nickel phosphide were observed (Fig. 3a). Swathing kamacite shows an enrichment in Co from the border (1.23 wt%) to the center (1.36 wt%, Table 1) of the rim. Metal has been partly replaced by iron hydroxides during terrestrial alteration.

Taenite grains mostly include plessite fields from  $0.1 \times 0.5$  to  $0.5 \times 1.5$  mm in size, comprising micro-Widmanstätten intergrowths of kamacite lamellae (Fig. 3b), 10–35  $\mu\text{m}$  in width, surrounded by high-Ni taenite bands 1–10  $\mu\text{m}$  in width. The lamellae occur as linear chains of kamacite lens-like grains each of which contains a nickel phosphide crystal in the core. Kamacite in the lamellae have lower Co content (0.9 wt%) than the swathing kamacite. Plessite fields have M-shaped profiles of Ni content from 15 wt% to 30 wt% in the border with taenite bands (Table 1).

Troilite forms rare spherical inclusions in olivine, 5–50  $\mu\text{m}$  in diameter. In several places, these troilite globules are grouped into linear chains. The troilite grains are connected with troilite veinlets in the fractured olivine. Troilite is partly replaced by iron hydroxides.

Olivine occurs as large fractured angular grains, 0.5–2 cm in size, and as rounded grains, up to 1 mm in size (Fig. 2). The fractures are filled by Fe,Ni hydroxide. Olivine borders with rare grains of chromite, low-Ca pyroxene, and Fe,Ni-metal <15  $\mu\text{m}$  in size (Fig. 3f).

Rarely olivine, up to 70  $\mu\text{m}$  in size, occurs between the pyroxene grains (Fig. 3c). Composition of the Karavannoe olivine is  $\text{Fa}_{19.5 \pm 1.09}$  (Table 2). Fayalite content of rounded olivine grains decreases from core  $\text{Fa}_{20.4}$  to rim  $\text{Fa}_{20}$  (Fig. 4a; Table S1 in supporting information). The rounded olivine grains are enriched in  $\text{Cr}_2\text{O}_3$  up to 0.8 wt% at the contact with chromite grains (Fig. 4b). In the large angular grains, the decrease in Fa content from the contact with metal to the core is less prominent (Fig. 4a; Table S1). However, large angular olivine grains show an increase in Cr content at the contact with small enclosed chromite inclusions, similar to that observed at the contact of rounded olivine and chromite grains (Fig. 4b; Table S1).

Low-Ca pyroxene occurs as large (Fig. 3c), up to 2 mm, or small, up to 30  $\mu\text{m}$ , grains located on the border of olivine and metal. Sometimes pyroxene forms a continuous rim along the margins of olivine grains at the contact with metal (Figs. 3d and 3e). Rare pyroxene inclusions of ~20  $\mu\text{m}$  in size are enclosed in olivine. Pyroxene composition is homogeneous and has average value  $\text{Fs}_{16.9}\text{Wo}_{0.6}$  (Fe/Mn = 57.3 atom%) (Table 2).

Phosphates in Karavannoe are represented by mostly xenomorphic grains of farringtonite ( $\text{Mg}_3[\text{PO}_4]_2$ ) and stanfieldite ( $\text{Ca}_4\text{Mg}_5[\text{PO}_4]_6$ ). Farringtonite, up to 70  $\mu\text{m}$  in size, occurs at the contact of the silicate assemblage with the metal and associates with low-Ca pyroxene, chromite, and metal (Fig. 3c). In some places, stanfieldite forms thick rims up to 50  $\mu\text{m}$  delineating low-Ca pyroxene. Some angular grains of stanfieldite, up to 40  $\mu\text{m}$  in size, are enclosed in low-Ca pyroxene (Fig. 3c). A large stanfieldite grain, up to 150  $\mu\text{m}$  in size, was found to be associated with nickel phosphide (Fig. 3d). Farringtonite contains 5 wt% of FeO and 42 wt% of MgO, whereas

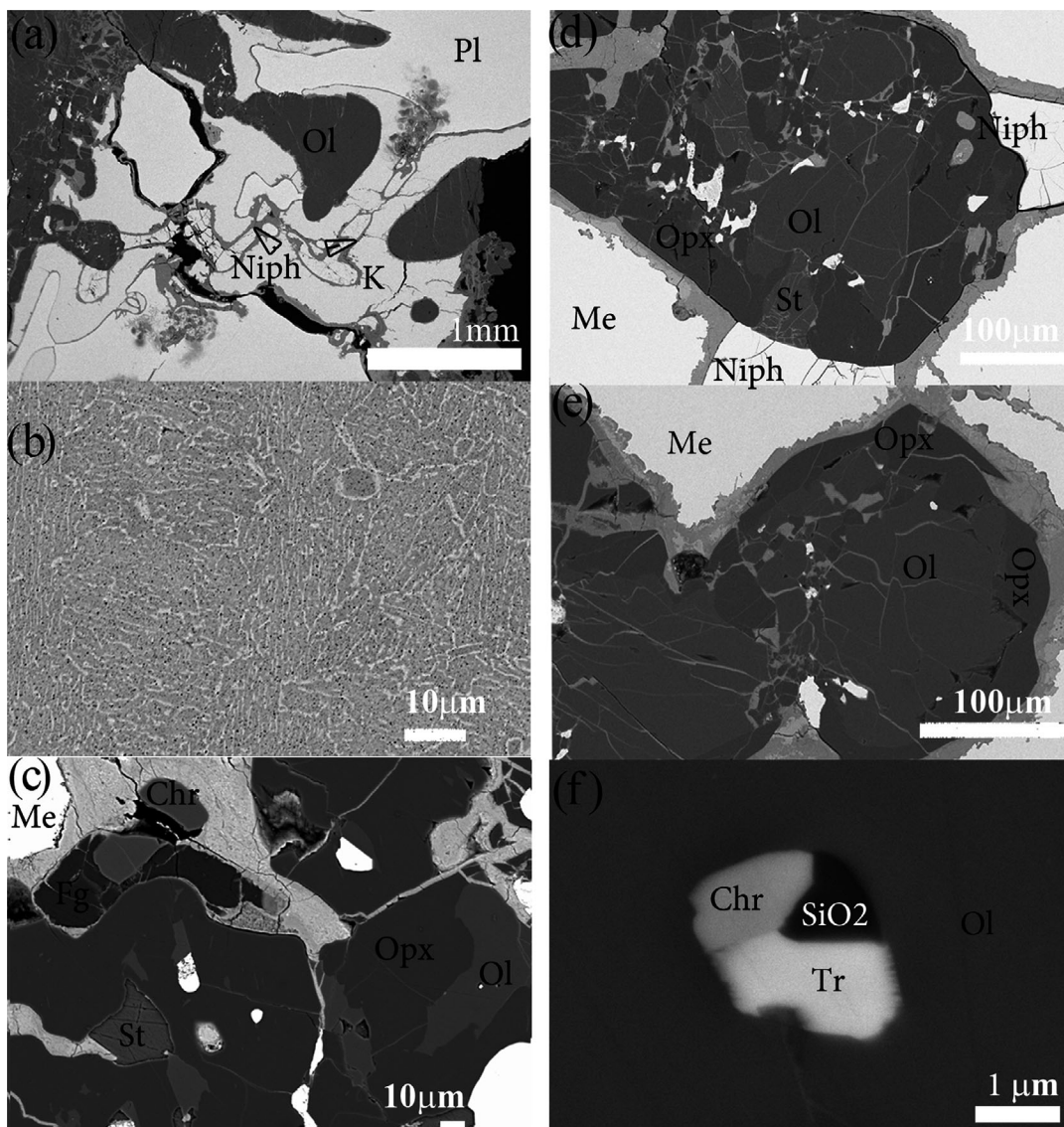


Fig. 3. BSE images of Karavannoe minerals: a) Nickel phosphide and kamacite in the metal. b) Micro-Widmanstätten intergrowths in the plessite areas consisting of the straight linear lamellae of low-Ni metal phase (“kamacite”) surrounded by high-Ni taenite bands. c) Orthopyroxene (Opx) crystals enclosing olivine (Ol) and stanfieldite (St), farringtonite (Fg), and chromite (Chr) at contacts between silicate crystals and metal. d) Isometric segregations of stanfieldite at the boundary between nickel phosphide rim with metal and olivine-orthopyroxene assemblage. e) Orthopyroxene (Opx) around olivine (Ol). f) Small chromite grain is in assemblage of troilite and silica enclosed in olivine.

stanfieldite contains 4.9 wt% of FeO, 20 wt% of MgO, and 26 wt% of CaO (Table 2).

Chromite occurs as large subhedral grains (100–300  $\mu\text{m}$ ) in metal and as rare small (<100  $\mu\text{m}$ ) inclusions in olivine. Large grains are chemically zoned. Profiles across these grains indicate that Mg/(Fe+Mg) and Al/(Al+Cr) ratios decrease from core to rim (from 28 to 18 and from 16 to 13, respectively) (Fig. 4c; Table S2 in supporting information), whereas TiO<sub>2</sub> and Cr<sub>2</sub>O<sub>3</sub> contents do not vary. Small chromite grains enclosed in olivine are shaped as clusters and linear

chains of subhedral isometric grains of 5–10  $\mu\text{m}$  in size. The Mg# of small chromite grains (16–29 atom%) is similar to that in the zoned large grain (Tables 2 and S2). One small chromite grain was observed in an assemblage with troilite and silica enclosed in olivine (Fig. 3f).

#### Trace Element Geochemistry of Olivine and Metal

Olivine has low contents of trace elements, near detection limits for Ca and Ti (Table 2), and REE

Table 1. Average chemical composition (wt%), standard deviation ( $\sigma$ ), and number of analyses ( $N$ ) of kamacite, taenite, and nickel phosphide from the Karavannoe pallasite.

Elements	Kamacite $N = 47$		Taenite $N = 57$		Nickel phosphide $N = 3$	
	Average	$\sigma$	Average	$\sigma$	Average	$\sigma$
Fe	89.4	1.5	75.2	3.90	39.3	2.5
P	0.18	0.04	0.17	0.04	0.36	0.04
Ni	7.50	0.48	24.4	4.30	45.5	0.4
Co	1.23	0.09	0.72	0.12	0.17	0.01
Cr	0.01	0.01	0.01	0.01	b.d.	
S	0.01	0.01	0.01	0.02	0.03	0.01
Total	98.4		100.5		99.4	
Formulae	$\text{Fe}_{0.91}\text{Ni}_{0.08}\text{Co}_{0.01}$		$\text{Fe}_{0.7}\text{Ni}_{0.3}$		$(\text{Ni}_{1.59}$ $\text{Fe}_{0.45})_{3.04}\text{P}_{0.95}$	

b.d. = below detection limit.

(Fig. 5). However, a weak prevalence of light rare earth element (LREE) over heavy rare earth element (HREE) was detected (LREE 0.0002–0.03, HREE 0.001–0.1  $\times$  CI).

Geochemistry data for the Karavannoe metal obtained by LA-ICP-MS and INAA (John Wasson, personal communication) are remarkably similar (Table 3). The difference of these data does not exceed 5% for Co, Ni, Cu, Sb, Ir, and Os; 8–15% for Rh, W, Re, Pt, and Au; and 30–50% for Ga, Ge, and As. The important differences are Cr and Ge contents. Chromium content obtained by LA-ICP-MS is below the detection level (1.2 ppm) in contrast with data obtained by INAA (1078 ppm), which may indicate the presence of chromite inclusions in the sample analyzed by INAA. A high Ge content in INAA analyses (130 ppm) obtained with 95% error limits for Ge of about  $\pm 12\%$  (Wasson, 2017) correlates with high Ga content (7 ppm) compared to LA-ICP-MS data (81 and 3.45 ppm, respectively); however, Ge/Ga ratios (23.5 and 18.6) are similarly high relative to the value (11) obtained by Hilton et al. (2020). The Ge/Ga ratios in Eagle Station (13.9) analyzed simultaneously with Karavannoe (Humayun et al., 2014) and Ge/Ga in Eagle Station (15) by Hilton et al. (2020) are similar. This could indicate that the differences in Ga and Ge abundances in Karavannoe obtained by our LA and INAA analyses and by Hilton et al. (2020) may not be a result of analytical errors and thus may reflect some heterogeneity of the investigated Karavannoe sample.

Figure 6 shows positive correlations of Os and Ir, Au and As, and W and Fe in ESPs including the Karavannoe pallasite. All ratios and concentrations were normalized to CI composition (Anders & Grevesse, 1989) and will be discussed further below.

## Oxygen Isotopic Compositions

Oxygen isotopic composition of olivine in the Karavannoe meteorite is  $\delta^{17}\text{O} = -6.25\text{‰}$ ;  $\delta^{18}\text{O} = -2.642\text{‰}$  and  $\Delta^{17}\text{O} = -4.878\text{‰}$  was previously published in Meteoritical Bulletin (<https://www.lpi.usra.edu/meteor/docs/mb101.pdf>) and Korochantsev et al. (2013). This is similar to the oxygen isotopic composition of CO/CV CCs and is located in the area of oxygen isotopic compositions of the other ES pallasites on the three-oxygen isotope diagram (Fig. 7) (Clayton & Mayeda, 1996).

## DISCUSSION

### Relationships of Karavannoe to the Eagle Station Pallasite Group and Other Types of Pallasites

The similarity of oxygen isotopic composition of Karavannoe to the other ES pallasites (Fig. 7) indicates that Karavannoe is a member of the ESP group. The oxygen isotope compositions of Karavannoe and ESPs are distinct from MG and pyroxene pallasites (Clayton & Mayeda, 1996) but are similar to that of bulk CO-CV chondrites (Fig. 7). Modal content of olivine in Karavannoe (60 vol%) is less than in other ES pallasites, 75–80 vol%, but in the range of the MG pallasites (35–85 vol%; Buseck & Holdsworth, 1977) and pyroxene pallasites (55–63 vol%; Mittlefehldt et al., 1998). The coarse olivine grains in Karavannoe are homogeneous ( $\text{Fa}_{19.5\pm 1.09}$  mole%) and similar to other members of the ESP group in being more ferrous than the olivine composition from the MG pallasites ( $\text{Fa}_{11-13}$ ; Boesenberg et al., 2012) and other pallasite groups (e.g., Wasson & Choi, 2003). The Fe/Mn ratio of the Karavannoe olivine ( $99 \pm 4$  atom%) is in the average range for ESPs (104; Mittlefehldt et al., 1998), but higher than the Fe/Mn ratio of the MG olivine (36–54; Mittlefehldt et al., 1998) and of the pyroxene pallasites' olivine (27; Mittlefehldt et al., 1998). Distribution of trace elements shows that olivine in Karavannoe as well as in other pallasites of the ESP and MG groups has the lowest REE abundances among meteoritic and terrestrial olivines (Hsu, 2003). However, the observed prevalence of LREE over HREE in some Karavannoe olivines, together with the high variability of REE concentrations between the different grains, may indicate the presence of captured melt inclusions or microinclusions of phosphates. We did not observe these directly, but an occurrence of rare small polymineral inclusions (Fig. 3f) could indicate that submicron captured melt inclusions may occur in olivine as well. Low-Ca pyroxene of Karavannoe by Wo content (0.6–1.0 mole%) corresponds to that of the ES pallasites and is similar to MG and pyroxene pallasites (Mittlefehldt et al., 1998).

Table 2. Average chemical composition (wt%), standard deviation ( $\sigma$ ), and number of analyses ( $N$ ) of olivine, pyroxene, phosphates, and chromite from the Karavannoe pallasite.

Elements	Olivine $N = 46$		Orthopyroxene $N = 10$		Farringtonite $N = 3$		Stanfieldite $N = 2$		Chromite $N = 35$	
	Average	$\sigma$	Average	$\sigma$	Average	$\sigma$	Average	$\sigma$	Average	$\sigma$
SiO <sub>2</sub>	38.9	0.4	56.9	0.5	n.d.	n.d.	n.d.	n.d.	0.02	b.d.
TiO <sub>2</sub>	b.d.	b.d.	0.03	b.d.	n.d.	n.d.	n.d.	n.d.	0.06	0.02
Al <sub>2</sub> O <sub>3</sub>	b.d.	b.d.	0.12	0.03	n.d.	n.d.	n.d.	n.d.	7.45	0.45
Cr <sub>2</sub> O <sub>3</sub>	0.12	0.21	0.09	0.04	n.d.	n.d.	n.d.	n.d.	61.4	0.5
FeO	18.7	0.9	11.4	0.2	5.03	0.1	4.94	0.14	25.9	1.2
MnO	0.19	0.01	0.2	0.03	0.11	0.02	0.31	0.02	0.35	0.04
MgO	42.1	1	31.8	0.5	42.1	0.7	20.4	0.03	4.67	0.71
CaO	b.d.	b.d.	0.3	0.11	0.03	b.d.	26.4	n.d.	n.d.	n.d.
Na <sub>2</sub> O	n.d.	n.d.	b.d.	b.d.	n.d.	n.d.	n.d.	n.d.	n.d.	n.d.
K <sub>2</sub> O	n.d.	n.d.	b.d.	b.d.	n.d.	n.d.	n.d.	n.d.	n.d.	n.d.
P <sub>2</sub> O <sub>5</sub>	n.d.	n.d.	n.d.	n.d.	51.9	0.2	48.5	0.45	n.d.	n.d.
NiO	0.01	0.01	0.04	0.02	n.d.	n.d.	n.d.	n.d.	b.d.	b.d.
V <sub>2</sub> O <sub>3</sub>	n.d.	n.d.	n.d.	n.d.	n.d.	n.d.	n.d.	n.d.	0.59	0.04
Total	100	0.5	100.8	0.6	99.2	0.7	100.6	0.53	100.5	0.56
Fa	20									
Fs	–		16.9							
Wo	–		0.6							
En	–		82.6							
*Mg# %	80		83						24.3	
Fe/Mn atomic.	98.8		57.3						74.1	
Formulae	Mg <sub>1.6</sub> Fe <sub>0.4</sub> (SiO <sub>4</sub> )		Mg <sub>1.66</sub> Fe <sub>0.33</sub> (SiO <sub>3</sub> ) <sub>2</sub>		Mg <sub>2.84</sub> Fe <sub>0.19</sub> (PO <sub>4</sub> ) <sub>2</sub>		Ca <sub>4.07</sub> Mg <sub>4.39</sub> Fe <sub>0.61</sub> (PO <sub>4</sub> ) <sub>6</sub>		Fe <sub>0.75</sub> Mg <sub>0.24</sub> Cr <sub>0.68</sub> Al <sub>0.3</sub> V <sub>0.02</sub> O <sub>4</sub>	

n.d. = not determined; b.d. = below detection limit 0.01; \*Mg# =  $100 \times \text{Mg}/(\text{Fe}+\text{Mg})$ , atomic%.

Although a high-Ca pyroxene (Wo<sub>45</sub>Fs<sub>7</sub>) was reported in the ESP group (Davis & Olsen, 1991), it was not observed in Karavannoe.

Phosphate compositions are similar to those of ESPs and the MG pallasite Springwater (Hsu, 2003). Farringtonite and stanfieldite should crystallize from a melt after olivine, orthopyroxene, and chromite, at 1350–1100 °C according to the Mg<sub>3</sub>(PO<sub>4</sub>)<sub>2</sub>-Ca<sub>3</sub>(PO<sub>4</sub>)<sub>2</sub> diagram (Ando, 1958). Based on our Karavannoe observations and experimental data, stanfieldite can be regarded as a late-stage cumulate of silicate-phosphate melts (Tollari et al., 2006). The texture of intergrowth of stanfieldite (Figs. 3c and 3d) with enstatite and orthopyroxene with coexisting nickel phosphide indicates an absence of reaction relationships and argues against the possible metamorphic origin of phosphates from the olivine due to oxidation of metal and/or phosphides proposed by Davis and Olsen (1991) or by interaction between silicate and metallic reservoirs in the MG parent planetesimal, with phosphorous, chromium, and oxygen sourced from the metallic liquid (McKibbin et al., 2019). Based on these observations, we propose that olivine-orthopyroxene-phosphate intergrowth, polymineral microinclusions, and relative LREE enrichment of olivine could be a result of crystallization of the late melt remaining after fractional crystallization of the olivine, or could be a portion of partial melt captured by olivine restite segregated from the partially molten source.

Like olivine, chromite in Karavannoe is more ferrous (Mg# 24) than chromite from the MG pallasites (Mg# 26–43; Boesenberg et al., 2012).

Karavannoe's coarse irregular angular olivine grains are uniform in composition, have no zoning, and are fragments of even larger olivine crystals that could be an indicator of fragmentation during addition of metal similar to those observed in other pallasites of various groups (Buseck & Goldstain, 1969; Scott, 1977a).

In contrast, Karavannoe's small round grains of olivine and chromite have a magmatic-like zoning (Mg-rich core and Fe-rich rim). This zoning could not be formed during the type of grain boundary migration proposed by Scott (1977a) to explain the origin of the rounded olivines in the pallasites. The zoning also appears not to be a result of mineral grain exchange with metal, but could indicate rapid crystallization of small silicate melt droplets floating in liquid metal. The melt could be formed from the silicate material remelted during the process, which brought silicates and metal together, or through partial melting of pallasite material in some late heating event.

During crystallization of the growing crystals of the second generation, their compositions were not equilibrated with the liquid, resulting in heterogeneous distribution of FeO and MgO (Figs. 4a–c). Thus, the melting event likely was impact-related, occurring in situ due to propagation of the shock wave followed by postshock melting. Alternatively, the impact metal-

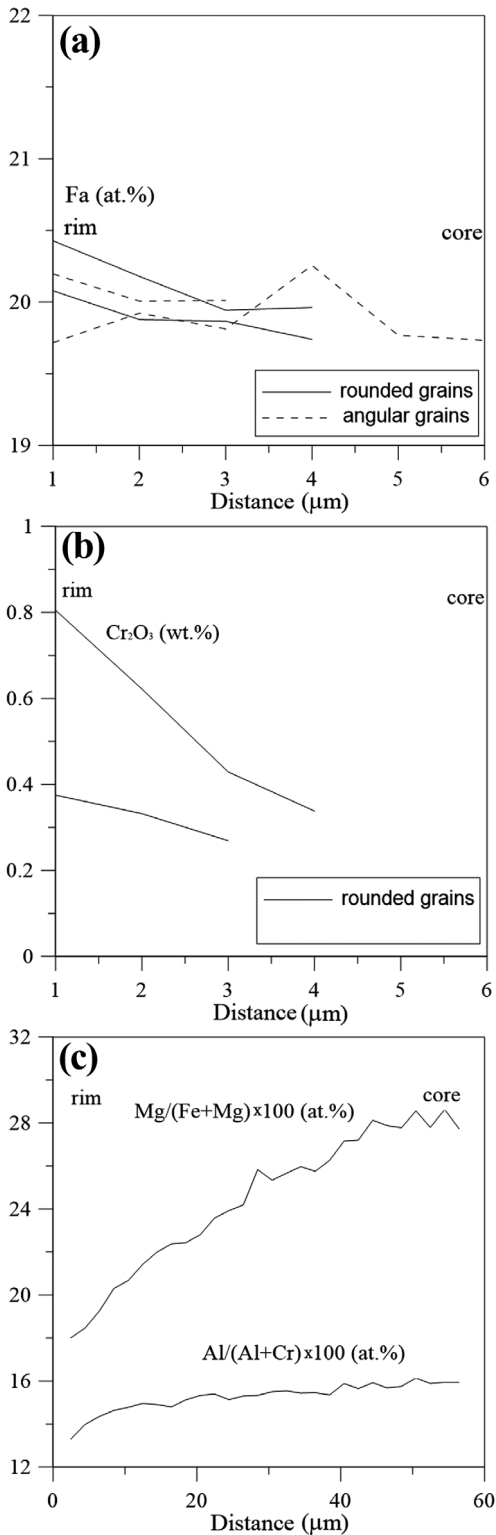


Fig. 4. a)  $\text{Fe}/(\text{Mg}+\text{Fe}) \times 100$  (atom%) and (b)  $\text{Cr}_2\text{O}_3$  wt% profiles from core to rim of olivine grains in Karavannoe; (c) profiles from core to rim of chromite grains in Karavannoe showing  $\text{Mg}/(\text{Mg}+\text{Fe}) \times 100$  and  $\text{Al}/(\text{Cr}+\text{Al}) \times 100$  in atomic ratios.

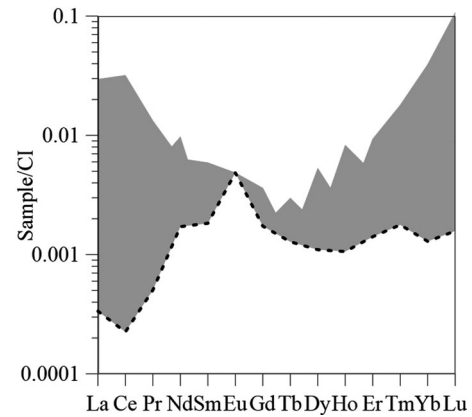


Fig. 5. Variations of the REE patterns (gray fill) and their detection limits (dashed line) for olivine from Karavannoe pallasite. Data are CI-chondrite-normalized by Anders and Grevesse (1989).

silicate melt could have mixed with large olivine and/or olivine-metal fragments and crystallized relatively quickly.

The metal of the five ES pallasites is rich in Ni, Co, and Ge, and depleted in W and Ga (Fig. 8) relative to the metal of the MG (Hilton et al., 2020; McCoy et al., 2019; Scott, 1977a; Wasson & Choi, 2003). However, variation in highly siderophile element (HSE) in members of ESP could be an indicator of fractional crystallization of the metal.

The Karavannoe metal has a nearly chondritic Co/Ni ratio, similar to the Eagle Station and Cold Bay pallasites (Humayun & Weiss, 2011), and its trace element geochemistry indicates that it is a product of fractional crystallization of a metallic liquid (based on abundances of Re, Os, and Ir) similar to that observed in the magmatic groups of iron meteorites (Fig. 6). We plotted the ESP data together with composition of the magmatic groups of iron meteorites such as IVB (Fig. 6a). The positive linear trend of the Os/Ir ratio in Karavannoe, Cold Bay, and Eagle Station (Fig. 6a) has a smaller slope than the trend in chondrites (Os/Ir ~1), which may indicate fractional crystallization of the metal melt. Since both Os and Ir are compatible with the solid phase, but Os is preferentially distributed into solid metal ( $D_{\text{Os}} > D_{\text{Ir}}$ , where  $D$  is the solid metal/liquid metal distribution coefficient), the positive linear trend for the Os/Ir ratio has a smaller slope than in chondrites, where the Os/Ir ratio is ~ 1 (Anders & Grevesse, 1989; Campbell et al., 2002).

The positive Au-As trend (Fig. 5b) observed in Karavannoe and other ESPs suggests a magmatic origin similar to the IIAB, IIIAB, IIF, and IVA groups of iron meteorites. The incompatible elements Au and As are usually well correlated during melting and fractional



Table 3. Siderophile element abundances (ppm) of the Karavannoe metal obtained by LA-ICP-MS analyses, the bulk composition obtained by the INAA, and the bulk composition of CV- and CO-derived model metallic liquids.

Elements	LA-ICP-MS (raster)	LA-ICP-MS (raster)	LA-ICP-MS (raster)	LA-ICP-MS (raster)	LA-ICP-MS (average)	LA-ICP-MS detection limits	(INAA) *	CV-derived model metal liquid	CO-derived model metal liquid
P	727	723	742	777	742	2	n.d.		
Cr	2	1	1	1	1	0.5	1078		
Fe	804000	823000	816000	803000	812000		n.d.	824684	842036
Co	8170	8520	8120	7960	8190		8030	6697	7321
Ni	167000	163000	172000	173000	169000		174000	149320	148970
Cu	300	289	301	313	301	0.2	292	1115	1330
Ga	3.54	3.38	3.22	3.66	3.45	0.01	7	40.16	14.75
Ge	80	85	77	83	81	0.05	130	188	223
As	10.7	11.4	9.23	10.3	10.4	0.003	14.5	17.8	20.7
Mo	14.6	16.5	16.2	15.5	15.7	0.07	n.d.	23.1	20.2
Ru	15.8	17	16.6	16.1	16.4	0.007	14.2	11.2	11.6
Rh	2.22	2.42	2.32	2.23	2.3	0.002	n.d.	1.9	1.9
Pd	5.89	6.01	6.17	6.16	6.06	0.007	n.d.	7.86	7.48
Sn	0.33	0.28	0.22	0.32	0.29	0.03	n.d.	10.04	9.47
Sb	0.3	0.28	0.25	0.31	0.29	0.002	0.27	0.95	1.12
W	0.25	0.28	0.27	0.27	0.27	0.001	0.29	0.21	0.33
Re	0.79	0.91	0.87	0.82	0.85	0.0002	0.94	0.67	0.59
Os	9.7	11.3	10.5	10.1	10.4	0.0007	11	8.35	8.41
Ir	8.99	10.3	9.63	9.33	9.55	0.0003	9.82	7.85	7.82
Pt	18.2	20.3	19.4	18.9	19.2	0.004	17.2	15.17	12.77
Au	1.32	1.37	1.36	1.39	1.36	0.001	1.48	1.61	1.96

D.L. = detection limit.

\*Data from personal communication with John Wasson.

crystallization processes. This correlation is a result of stepwise enrichment of the metal liquid by the siderophile elements with solid/liquid distribution coefficients  $<1$  during crystallization of the Fe,Ni crystals (Chabot et al., 2003). The ESP metal composition is plotted with the CV metal and CV bulk composition trends (Fig. 6c). The W/Ni ratio of Karavannoe metal is lower than that of bulk CV and CO compositions, indicating that if the ESP metal originated from CV or CO material, the source should be depleted in tungsten before complete melting, probably due to its removal as  $WO_2$  together with volatile outflow during parent body heating (e.g., Krot et al., 2004).

### Melting Model for Metal from the Eagle Station Pallasites

A link between ESP meteorites and CV chondrites was suggested based upon oxygen isotopic composition (Clayton & Mayeda, 1996) and some similarities of siderophile element geochemistry (Carpornzen et al., 2011; Humayun et al., 2014; Humayun & Weiss, 2011). Humayun and Weiss (2011) proposed that the chemical composition of ESPs may be plausibly derived by differentiation of CV (oxidized), CO, or CK chondrites. Hilton et al. (2020) showed that ESPs, including

Karavannoe, have HSE abundances (Re, Os, Ir, Ru, Pt, and Pd) of metal that are consistent with metal formation in planetesimal cores by fractional crystallization with plausible links to the IIF irons, a member of the CC group based on Mo isotopes (Kruijer et al., 2017). However, IIF irons were formed under different redox condition than the ESP group, and they have a different trend on the plot W/Ni versus Fe/Ni (Fig. 6c). The metal compositions of the ESPs are different and if ESPs originate from a single primitive source, this could be a product of fractional crystallization of melt. The ESP olivine appears likely to be a product of large-scale igneous fractionation, pointing to the parent body interior as the formation region for ESPs.

To test the hypothesis of the origin of ESPs from CV, CO, and CK chondrite composition parent bodies, a model of fractional crystallization of metal from an initially completely molten chondrite source was constructed. In this model, the composition of the metal liquid was obtained by metal-silicate partitioning.

The composition of the model metallic melt was compiled from the average bulk compositions of CV chondrites for Fe, Co, Ni, S (Jarosewich, 1990); Cu, Ga, Ge, As, Mo, Pd, Sb, Sn, W, Au (Wasson & Kallemeyn, 1988); Ru, Rh, Pt (Fischer-Gödde et al.,

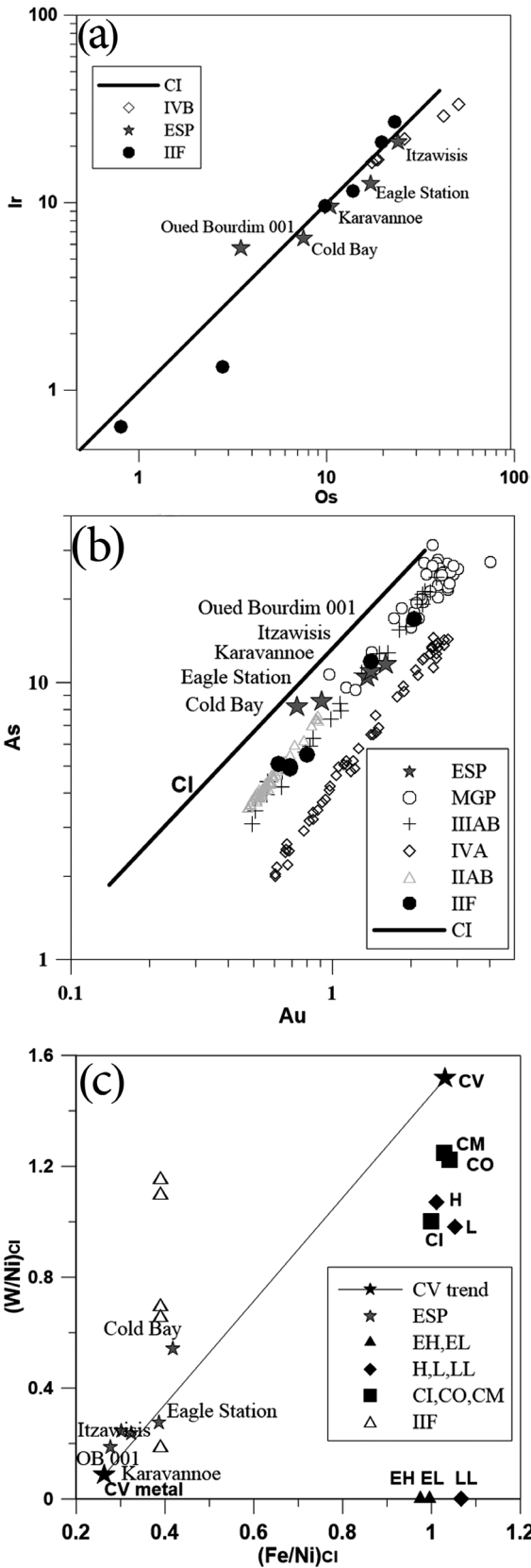


Fig. 6. a) Positive correlation of Os-Ir in Karavannoe, Eagle Station, Cold Bay and magmatic IVB irons. b) Magmatic correlation of Au-As in ESPs and magmatic IIAB irons, IIIAB, IIF, and IVA. c)  $(W/Ni)_{CI}$  versus  $(Fe/Ni)_{CI}$  in Karavannoe compared to other ESPs, metal of the CV chondrite composition, and bulk chondrites (H, L, LL, EL, EH, CI, CM, CV, CO). Data for Karavannoe (Kar.)—this study, Eagle Station (ES) and Cold Bay (CB) (Humayun & Weiss, 2011), MGP (Wasson & Choi, 2003), magmatic IVB irons (Campbell & Humayun, 2005), magmatic IIAB irons (Wasson et al., 2007), magmatic IIIAB irons (Wasson, 1999), magmatic IIF irons (Hilton et al., 2020), magmatic IVA irons (Wasson & Richardson, 2001), metal of CV chondrite composition (Humayun & Weiss, 2011; see text for details), and chondrites (Wasson & Kallemeyn, 1988).

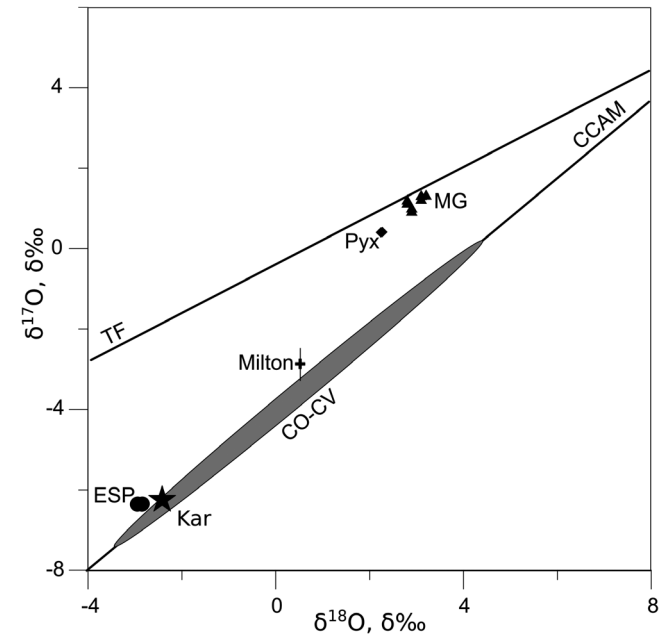


Fig. 7. Bulk oxygen isotopic composition of the Karavannoe olivine ( $\text{‰}$ ) compared to oxygen isotopic compositions of the Main Group (MG) and Eagle Station (ESP) pallasites (Clayton & Mayeda, 1978), the pyroxene pallasites (Pyx)—Vermillion and Yamato 8451 (Clayton & Mayeda, 1996) and the unique pallasite Milton (McCoy et al., 2019). TF = terrestrial fractionation line; CCAM = carbonaceous chondrite anhydrous mineral line (Clayton et al., 1977; Clayton & Mayeda, 1999). The analytical uncertainty is within symbol sizes—for ESP group  $\delta^{18}O$ —0.1 $\text{‰}$ ,  $\delta^{17}O$ —0.2 $\text{‰}$ ; for Karavannoe  $\delta^{18}O$ —0.08 $\text{‰}$ ,  $\delta^{17}O$ —0.04 $\text{‰}$ ; for Milton  $\delta^{18}O$ —0.2 $\text{‰}$ ,  $\delta^{17}O$ —0.7 $\text{‰}$ .

2010); and Re, Os, Ir (Horan et al., 2003). We assumed the distribution of Co, Ni, Ga, Ge, Mo, and W in the metal phase according to the metal/silicate distribution coefficients by Schmitt et al. (1989) under  $fO_2 = -10.8$  at 1300 °C, corresponding to IW and almost complete

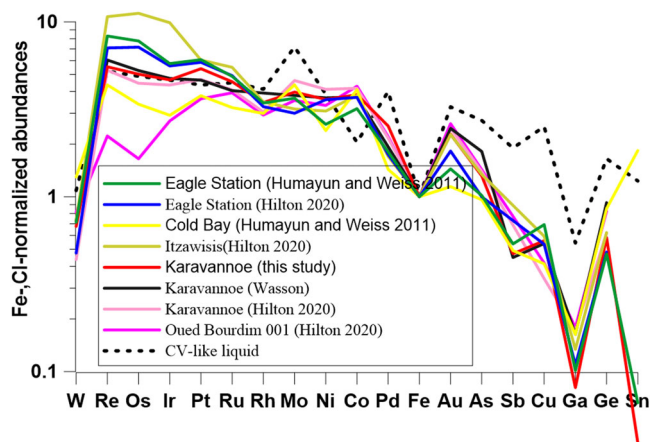


Fig. 8. Fe-, CI-chondrite-normalized average siderophile element abundances of five Eagle Station pallasites (ESP) determined by LA-ICP-MS compared to the CV-derived model metal liquid. (Color figure can be viewed at [wileyonlinelibrary.com](http://wileyonlinelibrary.com).)

distribution of other trace siderophiles into the metal. The average CV3 chondrite carbon content is  $0.73 \pm 0.45$  wt% (0.27–1.5 wt%; Jarosewich, 1990; Pearson et al., 2006). Carbon reacting with Fe affects the amount of reduced Fe and thus the amount of Ni in the metal liquid. In our model, all carbon (1.55 wt%) reacts with FeO to form CO gas and Fe metal during the melting of the chondrite source. To crystallize a Karavannoe-like metal with 16.8 wt% Ni, the initial melt should have ~15% Ni. Because Karavannoe contains only accessory troilite, we have proposed that all FeS melt would be removed from the system during the parent body internal heating but before complete melting of the CV-like material. Based on the assumptions above, the model calculations indicate that a CV-like material could produce a metal liquid with 16.8 wt%, containing ~1.55 wt% of carbon. The remaining silicate liquid has Mg/Fe mass ratio of 0.97, equivalent to ~Fo70. However, Karavannoe's actual olivine composition is Fo<sub>80</sub> and we cannot directly match our calculated compositions with this observation (see the Discussion section).

To model crystallization of the calculated metal liquid resulting from melting of the proposed CV chondrite source, we used the Rayleigh equation describing fractional crystallization, together with experimentally determined metal solid/liquid distribution coefficients (Chabot et al., 2003, 2009). These calculations (Fig. 9) predict a metallic solid consistent with an ESP composition, with the notable exception of Rh, Ru, Mo, Cu, Sb, and Ga. Crystallization of the first solid metal from the parental metallic liquid after 1–5% fractional crystallization ( $F = 1$ ) and 20% ( $F = 0.8$ ) provides the best fit with the Itzawisis and Eagle Station

compositions, respectively. Karavannoe, Cold Bay, and Qued Bourdim 001 require 50% ( $F = 0.5$ ), 60% ( $F = 0.4$ ), and 70% ( $F = 0.3$ ) fractional crystallization, respectively. Therefore, these results are comparable with those obtained in Hilton et al. (2020), but they are more delayed and show more clear differences between the crystallization path of ESP members.

The model metal liquid derived from a modified CV-like chondrite composition shares many characteristics of the Karavannoe metal composition, including the sloped refractory siderophile element pattern, and Ga depletion (Fig. 9). The model compositions are rich in Mo compared to ESPs, probably because molybdenum should be partially distributed into the escaping sulfide-rich melt but we did not calculate this effect. Depletion of ESPs in moderate (Cu) and highly volatile siderophiles could be interpreted as a result of later reheating of the fractionated metal in an open system. Depletion of Rh, Ru, and Mo could be a result of separation of phosphide liquid from the main mass of ESP precursor metal (0.27–1.5 wt%; Jarosewich, 1990; Pearson et al., 2006).

The bulk composition of CO chondrite-derived metal melt (Table 3) was calculated based on data by Wasson and Kallemeyn (1988) and Jarosewich (1990) to test a hypothesis about a possible genetic link between ESPs and CO CCs. Based on the approach and initial assumptions which we used for our CV metal liquid composition calculations, we have obtained a composition similar to a CO-like model metal liquid. Because CO chondrites are richer in Fe metal (up to 4.5 wt%) and poor in C (0.06–0.5 wt%; Jarosewich, 1990), more reduced than CV chondrites, to produce a metal liquid with 14.9 wt% Ni, a low carbon content (0.38 wt%) with Fe metal content of 3.07 wt% should be assumed in the starting CO composition. Thus, for a CO-like chondrite to be a feasible source of the ESP metal, the CO starting material should be ~7× enriched in carbon compared to known CVs. The model CO-derived metal liquid (Table 3) and the solid fraction of its 50% fractional crystallization are similar to the CV-derived calculated model liquids (Fig. 9b).

### Formation of Karavannoe and the Eagle Station Pallasite Group

Our modeling shows that the metal formed during the fractional crystallization of a CV-like metallic liquid has many characteristics of Karavannoe and the metal from other ESPs. Based on the model, Itzawisis, Eagle Station, Karavannoe, Cold Bay, and Qued Bourdim 001 could be produced as solids crystallized from a CV- or CO-like metallic liquid after ~1%, 1%, 40%, 50%, and 75% degree of fractional crystallization, respectively.

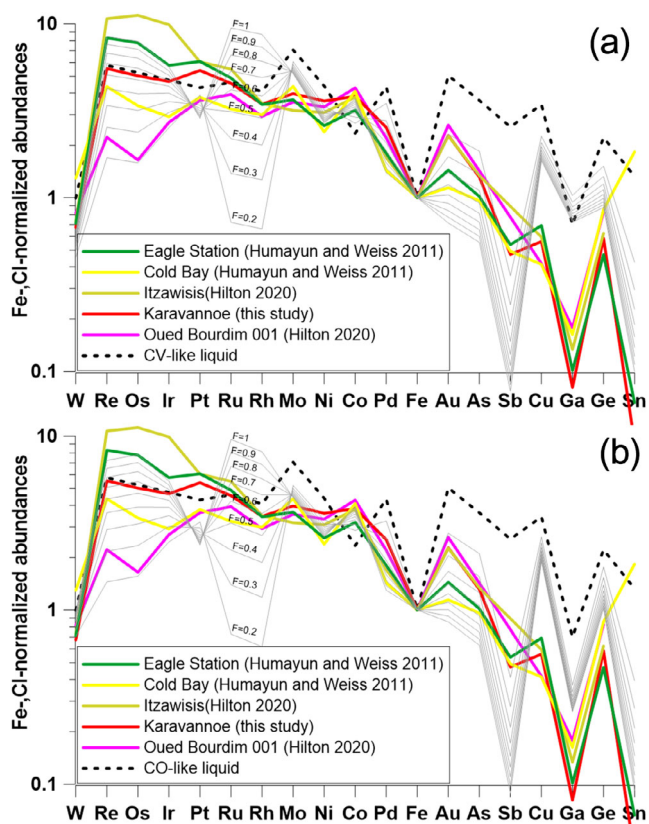


Fig. 9. Siderophile element pattern of five Eagle Station pallasites (ESP) and the calculated solid metal composition obtained: (a) from the CV-derived model metal liquid ( $F$  = fraction of the residual liquid); (b) from the CO-derived model metal liquid (Table 3). (Color figure can be viewed at [wileyonlinelibrary.com](http://wileyonlinelibrary.com).)

Itzawisis does not plot on the diagram at the first solid because it is enriched in siderophile elements, but its Ni content does correspond to the first solid formed in the model. Thus, during inward crystallization of the parent body core (see review in Abrahams & Nimmo, 2019), the Itzawisis and Eagle Station metals could be formed in the core near the contact with the olivine mantle while Cold Bay and Qued Bourdim 001 metals could represent deeper material of the core of the ESP parent asteroid, assuming that crystallization progressed from the edge to the center of the core.

However, when modeling CV chondrite-like material, the assumed reduction of FeO to Fe by reaction with carbon is pressure-sensitive because it produces a CO gas. The pressure of CO must be higher than the maximum internal pressure in the parent body interior, which sets a limit on size of the parent body. At a given  $T$  (1300 °C) and  $fO_2$  ( $-10.8$  or IW), carbon stability is limited by a pressure of  $\sim 100$  bar (Keppler & Golabek, 2019), which corresponds to the pressure in

the center of an ideal sphere (Warren, 2012) of CV or CO density ( $2.8$  and  $3.0$  g cm $^{-3}$ ; Flynn et al., 1999) of  $\sim 100$  km in radius (core radius 27 km). For a larger body, reduction of iron from the melt by carbon in the central part of the body will be suppressed by internal pressure and the resulting metal liquid will have Ni content higher than needed to crystallize the metal of Karavannoe using our model. The already reduced CO chondrite-like source, poor in carbon, does not act as a limiting factor on parent body size.

As noted above, the melting of a CV source could not produce the silicate complement of a metal melt similar in Mg# to the ESPs' olivine. We propose that melting of a CV bulk composition initially produced silicate liquid with a bulk composition corresponding to Fo $_{70}$  and metal containing  $\sim 15$  wt% of Ni. The Fo $_{80}$  olivine, which occurs in Karavannoe and ESPs, is not in equilibrium with the metal and could have been a product of the late evolutionary processes in the Karavannoe parent body mantle. In this scenario, early magnesium-rich olivine could have crystallized from the melt, settled down, and formed a basal layer of the ESP parent body mantle.

Our data suggest that the cooling of the metal-olivine rock was fast enough to record aspects of the parent taenites, including the small grain size (2–3 mm), Mg#, Cr $_2$ O $_3$  diffusional zoning observed in olivine grains, and Mg# zoning in chromite grains. The observed coexistence of large fragmented and small rounded olivine grains surrounded by metal crystallized from a melt could indicate that small olivine grains were remelted during the metal-silicate mixing process. The micro-Widmanstätten structure of the main metal mass and swathing low-Ni metal (kamacite) rimming the olivine indicate that slow subsolidus cooling below 600 °C (Yang et al., 1996) of the metal-olivine mixture occurred. It is difficult to apply the metallographic cooling rate models developed for iron meteorite groups to Karavannoe metal, because tetrataenite and cloudy taenite zone regions were not found. In addition, it is not certain if the Karavannoe Widmanstätten patterns formed from single crystals of taenite. Also, taenite grain boundaries and impingement effects by adjacent kamacite plates were absent.

Overall, the metal and silicates of Karavannoe indicate reheating, partial remelting, and quick crystallization, possibly due to cooling in a near-surface region of the parent body.

If Karavannoe and the ESPs had a common formation process, then it should be a mechanism that plausibly combines the processes of mixture of a metal formed at some intermediate stage of fractional crystallization with solid olivine from the mantle, quick cooling of the metal-silicate mixture during

crystallization at a high temperature, and slower subsolidus cooling. Because Karavannoe was reheated and partially melted during the final stage of its parent-body history, it lost many of the pristine textural features of its formation. Thus, it is unknown how and when the metal and olivine were mixed. Did the metal and olivine associate deep inside the parent body, or were these components combined as melt breccia on the surface? The models of collisions of separate silicate and metal bodies noted in the Introduction section appear to be poorly consistent with ESP genesis, because the models do not give the observed uniform silicate composition of ESP olivine. The models of a single parent body for metal and silicates assume various types of material transport between the core and the mantle within the parent body, and seem to be more likely for the genesis of the ESPs.

A ferrovolcanism model for the origin of the pallasites was presented by Johnson et al. (2020). It describes the pallasite formation as intrusions of sulfur-rich metal melt formed in the late stages of core crystallization into an olivine-rich mantle, driven by excess pressure. This mechanism explained the general low S content in pallasites, but faces a challenge for explaining ESP genesis because ESPs' fractionated metal differs in composition from the late Ni and S-rich liquids suggested in this mechanism.

Hilton et al. (2020) suggested a pallasite origin mechanism involving an impact to transfer the olivine into the liquid core where it must be isolated by a quickly solidified outer core shell and then stepwise captured by crystallizing inward metal. Hilton et al. (2020) did not report the details of the proposed impact injection of olivine into the liquid metal core, but it should be a result of near-complete excavation of the mantle, because the basement of impact craters formed in silicate mantle is expected to have a fractured blocky zone degrading with depth (Melosh, 1989). In a high velocity impact, liquid behaves like a solid body and the excavated material moves out of the crater, so large-scale injection of olivine from the fractured crater basement to the liquid metal beneath the crater seems unlikely. According to the model by Hilton et al. (2020), enough olivine should enter the core to provide a high olivine–metal ratio throughout the fractional crystallization process. Our results indicate that the metal of some ESPs was formed by up to 50% fractional crystallization. Therefore, up to this stage, the crystallization front should leave behind the same amount of olivine crystals as ahead of the front to form pallasites with different metal composition, which appears unlikely.

Other authors (Carpörzen et al., 2011; Hsu, 2003; Elkins-Tanton et al., 2011; Tarduno et al., 2014) consider that pallasites have not necessarily formed at

the mantle–core boundary of their parent bodies and based on the pallasite thermal histories, they may have formed at a shallow depth and were subsequently buried deep under a regolith blanket.

As an alternative mechanism of ESP genesis, we propose that during a large-scale impact, large long fractures could have formed in the basement of a crater which excavated deep mantle (Figs. 10a and 10b). The fractures propagated through the basal mantle layer and reached the molten core, and were then filled by unfractionated metal during the relaxation of the crater bottom. Due to heat loss through the crater bottom, the fractional crystallization would progress downward from the intrusion into the parent body, resulting in the association of olivine of uniform composition captured by metal from the intrusion walls forming the metal of different composition. In this model, the ESPs could represent different parts of an intrusion exposed by later impact(s). In this case, IIF irons possibly related to ESPs (Hilton et al., 2020) could represent the inner parts of intrusions poor in olivine. In addition, olivine could be mixed with metal from different intrusion layers during later impact(s) on the surface of the parent body.

In any ESP genesis scenario, the parent body should then be significantly disrupted to expose core–mantle material. Since our observations of Karavannoe indicate reheating, remelting, and quick cooling, we suggest that after the catastrophic disruption of the ESP parent body, an offspring body composed of pallasite material then underwent small-scale impact. Karavannoe could then form by impact melting of pallasite material followed by rapid crystallization of the resulting metal melt matrix breccia and its relatively slow subsolidus cooling under a thermal insulation blanket of reaccruting crater ejecta material.

## CONCLUSION

The Karavannoe pallasite belongs to the ESP group based on oxygen isotopic compositions, mineralogy, and geochemistry of siderophile elements. Ratios of Re, Os, Ir, and the positive Au–As trend observed in Karavannoe and other members of the ESP group indicate fractionation similar to that observed in the magmatic groups of iron meteorites. Low W and Ga and high Ni and Co contents of the metal associated with ferrous olivine in ESPs indicate an oxidized primitive precursor material of their parent body.

Our calculations suggest that the precursor material of Karavannoe and other ESP metal may have CV or CO chondrite-like composition, supporting the early conclusions of Humayun and Weiss (2011) and Humayun et al. (2014). Metal of the Karavannoe

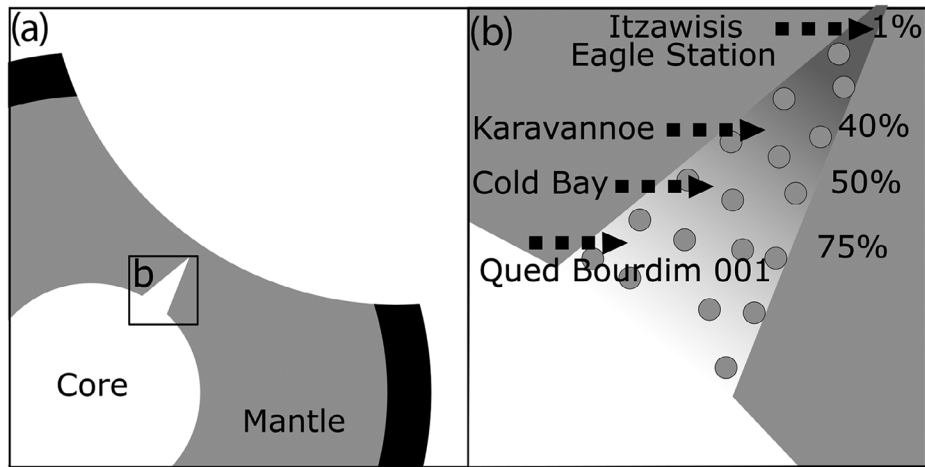


Fig. 10. A mechanism of the Eagle Station pallasite genesis: (a) the large-scale impact excavated the deep mantle of the ESP parent body. The fractures propagating through the basal mantle layer reach the molten core. The fractures were filled by unfractionated metal during the relaxation of the crater bottom; (b) due to a heat loss through the crater bottom, the fractional crystallization progresses from up to down of the intrusion inward the parent body resulting in association of olivine of the uniform composition captured by metal from the walls of intrusion forming the metal of different composition.

composition could form from CV- or CO-derived model metal liquids after ~50% fractional crystallization and removal of early formed solid metal crystals, while the olivine should represent evolved mantle material. For a CV-like source, the ESP parent body should not be larger than 200 km in diameter, limited by internal pressure suppressing the reduction of FeO by carbon. Based on our results and previous studies of ESPs, we propose that Karavannoe and other ESPs could have formed by fractional crystallization of liquid metal intrusion injected into mantle fractures as a result of a large-scale impact event exposing a deep mantle layer, cooling through the crater bottom and fractionally crystallizing downward, capturing olivines from the intrusion walls. Different parts of the intrusion could be segregated as ESPs by multiple further impacts or due to disruption of the ESP parent body into smaller offspring. It is also possible that Karavannoe was formed as a result of impact mixing of metal and olivine on the surface of one of the offspring bodies. The CV–ESP link established by our results provides important support for petrological, isotopic, and paleomagnetic evidence of a partially differentiated CV chondrite parent body (Aléon et al., 2020; Carporzen et al., 2011; Irving et al., 2004).

*Acknowledgments*—We greatly appreciate John Wasson for his generous help in obtaining INAA data for this meteorite. This work was partially (microprobe analyses and theoretical modeling) supported by a grant from the Russian Fund of Basic Research (#20-05-00117A) and by research theme of the Vernadsky Institute

(petrographic investigations and SEM study). This research was (partially) supported by the Program of Moscow State University Development. Research activities at Florida State University were supported by NASA grants (NNX13AI06G, #80NSSC18K0595) to Munir Humayun. The National High Magnetic Field Laboratory is supported by the National Science Foundation through NSF/DMR-1644779 and the state of Florida. We are grateful to Associated Editor Dr. A. Ruzicka and reviewers Dr. R. Ash and Dr. S. Goderis for help in improving the manuscript.

*Data Availability Statement*—Data available on request from the authors.

*Editorial Handling*—Dr. A. J. Timothy Jull

## REFERENCES

- Abrahams, J. N. H., and Nimmo, F. 2019. Ferrovulcanism: Iron Volcanism on Metallic Asteroids. *Geophysical Research Letters* 46: 5055–64.
- Agee, C. B., Ziegler, K., and Muttik, N. 2015. New Unique Pyroxene Pallasite: Northwest Africa 10019 (Abstract #5084). 78th Meteoritical Society Meeting.
- Aléon, J., Aléon-Toppani, A., Platevoet, B., Bardintzeff, J.-M., McKeegan, K. D., and Brisset, F. 2020. Alkali Magmatism on a Carbonaceous Chondrite Planetesimal. *Proceedings of the National Academy of Sciences* 117: 8353–9.
- Anders, E., and Grevesse, N. 1989. Abundances of the Elements: Meteoritic and Solar. *Geochimica et Cosmochimica Acta* 53: 197–214.

- Ando, J. 1958. Phase Diagrams of  $\text{Ca}_3(\text{PO}_4)_2\text{-Mg}_3(\text{PO}_4)_2$  and  $\text{Ca}_3(\text{PO}_4)_2\text{-CaNaPO}_4$  Systems. *Bulletin Chemical Society of Japan* 31: 201–5.
- Boesenber, J. S., Delaney, J. S., and Hewins, R. H. 2012. A Petrological and Chemical Reexamination of Main Group Pallasite Formation. *Geochimica et Cosmochimica Acta* 89: 134–58.
- Buchwald, V. F. 1975. *Handbook of Iron Meteorites. Their History, Distribution, Composition and Structure*. Berkeley: The University of California Press.
- Buseck, P. R., and Goldstain, J. I. 1969. Olivine Compositions and Cooling Rates of Pallasitic Meteorites. *Geological Society of America Bulletin* 80: 2141–58.
- Buseck, P. R., and Holdsworth, E. 1977. Phosphate Minerals in Pallasite Meteorites. *Mineralogical Magazine* 41: 91–102.
- Campbell, A. J., and Humayun, M. 1999. Trace Element Microanalysis in Iron Meteorites by Laser Ablation ICPMS. *Analytical Chemistry* 71: 939–46.
- Campbell, A. J., and Humayun, M. 2005. Compositions of Group IVB Iron Meteorites and Their Parent Melt. *Geochimica et Cosmochimica Acta* 69: 4733–44.
- Campbell, A. J., Humayun, M., and Weisberg, M. K. 2002. Siderophile Element Constraints on the Formation of Metal in the Metal-Rich Chondrites Bencubbin, Weatherford, and Gujba. *Geochimica et Cosmochimica Acta* 66: 647–60.
- Carporzen, L., Weiss, B. P., Elkins-Tanton, L. T., Shuster, D. L., Ebel, D. S., and Gattacceca, J. 2011. Magnetic Evidence for a Partially Differentiated Carbonaceous Chondrite Parent Body. *Proceedings of the National Academy of Sciences* 108: 6386–9.
- Chabot, N. L., Campbell, A. J., Jones, J. H., Humayun, M., and Agee, C. B. 2003. An Experimental Test of Henry's Law in Solid Metal Liquid Metal Systems with Implications for Iron Meteorites. *Meteoritics & Planetary Science* 38: 181–96.
- Chabot, N. L., Saslow, S. A., McDonough, W. F., and Jones, J. H. 2009. An Investigation of the Behavior of Cu and Cr During Iron Meteorite Crystallization. *Meteoritics & Planetary Science* 44: 505–19.
- Clayton, R. N., and Mayeda, T. K. 1978. Genetic Relations Between Iron and Stony Meteorites. *Earth and Planetary Science Letters* 40: 168–74.
- Clayton, R. N., and Mayeda, T. K. 1996. Oxygen Isotope Studies of Achondrites. *Geochimica et Cosmochimica Acta* 60: 1999–2018.
- Clayton, R. N., and Mayeda, T. K. 1999. Oxygen Isotope Studies of Carbonaceous Chondrites. *Geochimica et Cosmochimica Acta* 63: 2089–104.
- Clayton, R. N., Onuma, N., Grossman, L., and Mayeda, T. K. 1977. Distribution of the Pre-Solar Component in Allende and Other Carbonaceous Chondrites. *Earth and Planetary Science Letters* 34: 209–24.
- Davis, A. M., and Olsen, E. J. 1991. Phosphates in Pallasite Meteorites as Probes of Mantle Processes in Small Planetary Bodies. *Nature* 353: 637–40.
- Elkins-Tanton, L. T., Weiss, B. P., and Zuber, M. T. 2011. Chondrites as Samples of Differentiated Planetesimals. *Earth and Planetary Science Letters* 305: 1–10.
- Fischer-Gödde, M., Becker, H., and Wombacher, F. R. 2010. Rhodium, Gold and Other Highly Siderophile Element Abundances in Chondritic Meteorites. *Geochimica et Cosmochimica Acta* 74: 356–79.
- Flynn, G. J., Moore, L. B., and Klöck, W. 1999. Density and Porosity of Stone Meteorites: Implications for the Density, Porosity, Cratering, and Collisional Disruption of Asteroids. *Icarus* 142: 97–105.
- Gregory, J. D., Mayne, R. G., Boesenber, J. S., Humayun, M., Silver, A. P., Greenwood, R. C., and Franchi, I. A. 2016. Choteau Makes Three: A Characterization of the Third Member of the Vermillion Subgroup (Abstract #2393). 47th Lunar and Planetary Science Conference. CD-ROM.
- Hilton, C. D., Ash, R. D., and Walker, R. J. 2020. Crystallization Histories of the Group IIF Iron Meteorites and Eagle Station Pallasites. *Meteoritics & Planetary Science* 55: 2570–86.
- Horan, M. F., Walker, R. J., Morgan, J. W., Grossman, J. N., and Rubin, A. E. 2003. Highly Siderophile Elements in Chondrites. *Chemical Geology* 196: 5–20.
- Hsu, W. 2003. Minor Element Zoning and Trace Element Geochemistry of Pallasite. *Meteoritics & Planetary Science* 38: 1217–41.
- Humayun, M., Teplyakova, S. N., Lorenz, C. A., Ivanova, M. A., and Korochantsev, A. V. 2014. Siderophile Element Abundances in Karavannoe: Implication for the Origin of the Eagle Station Pallasites (Abstract #2293). 45th Lunar and Planetary Science Conference. CD-ROM.
- Humayun, M., and Weiss, B. P. 2011. A Common Parent Body for Eagle Station Pallasites and CV Chondrites (Abstract #1507). 42nd Lunar and Planetary Science Conference. CD-ROM.
- Irving, A. J., Larson, T. E., Longstaffe, F. J., Rumble, D., Bunch, T. E., Wittke, J. H., and Kuehner, S. M. 2004. A Primitive Achondrite with Oxygen Isotopic Affinities to CV Chondrites: Implications for Differentiation and Size of the CV Parent Body (Abstract #P31C-02). EOS Transactions AGU 85.
- Jarosewich, E. 1990. Chemical Analyses of Meteorites: A Compilation of Stony and Iron Meteorite Analyses. *Meteoritics* 25: 323–37.
- Johnson, B. C., Sori, M. M., and Evans, A. J. 2020. Ferrovolcanism on Metal Worlds and the Origin of Pallasites. *Nature Astronomy* 4: 1–4.
- Keppler, H., and Gobarek, G. 2019. Graphite Floatation on a Magma Ocean and the Fate of Carbon During Core Formation. *Geochemical Perspective Letters* 11: 12–7.
- Korochantsev, A. V., Lorenz, C. A., Ivanova, M. A., Teplyakova, S. N., Kononkova, N. N., Roshina, I. A., Borisovsky, S. E. et al. 2013. Karavannoe: A New Member of the Eagle Station Pallasite Group (Abstract #2020). 44th Lunar and Planetary Science Conference. CD-ROM.
- Kracher, A., Willis, J., and Wasson, J. T. 1980. Chemical Classification of Iron Meteorites IX: A New Group (IIF) Revision of IAB and IIICD, and Data on 57 Additional Irons. *Geochimica et Cosmochimica Acta* 44: 773–87.
- Krot, A. N., Petaev, M. I., and Bland, P. A. 2004. Multiple Formation Mechanisms of Ferrous Olivine in CV Carbonaceous Chondrites During Fluid-Assisted Metamorphism. *Antarctic Meteorite Research* 17: 153–71.
- Kruijer, T. S., Burkhardt, C., Budde, G., and Kleine, T. 2017. Age of Jupiter Inferred from the Distinct Genetics and Formation Times of Meteorites. *Proceedings of the National Academy of Sciences* 114: 201704461.
- Luu, T.-H., Chaussidon, M., and Birck, J.-L. 2014. Timing of Metal-Silicate Differentiation in the Eagle Station Pallasite Parent Body. *Comptes Rendus Geoscience* 346: 75–81.

- Malvin, D. J., Wasson, J. T., Clayton, R. N., Mayeda, T. K., and Curvello, W. S. 1985. Bocaiuva—A Silicate-Inclusion Bearing Iron Meteorite Related to the Eagle Station Pallasites. *Meteoritics* 20: 257–72.
- McCoy, T. J., Corrigan, C. M., Nagashima, K., Reynolds, V. S., Ash, R. D., McDonough, W. F., Yang, J., Goldstein, J. I., and Hilton, C. D. 2019. The Milton Pallasite and South Byron Trio Irons: Evidence for Oxidation and Core Crystallization. *Geochimica et Cosmochimica Acta* 259: 358–70.
- McKibbin, S. J., Pittarello, L., Makarona, C., Hamann, C., Hecht, L., Chernozhkin, S. M., Goderis, S., and Claeys, P. 2019. Petrogenesis of Main Group Pallasite Meteorites Based on Relationships Among Texture, Mineralogy, and Geochemistry. *Meteoritics & Planetary Science* 54: 2814–44.
- Melosh, H. J. 1989. *Impact Cratering. A Geological Process. Oxford Monographs on Geology and Geophysics No.11.* New York: Oxford University Press.
- Miller, M. F., Franchi, I. A., Sexton, A. S., and Pillinger, C. T. 1999. High Precision  $\Delta^{17}\text{O}$  Isotope Measurements of Oxygen from Silicates and Other Oxides: Method and Applications. *Rapid Communication on Mass Spectrometry* 13: 1211–7.
- Mittlefehldt, D., McCoy, T., Goodrich, C., and Kracher, A. 1998. Non-Chondritic Meteorites from Asteroidal Bodies. In *Planetary Materials*, edited by J. J. Papike, 4-1–4-195. Washington, D.C.: Mineralogical Society of America.
- Pearson, V. K., Sephton, M. A., Franchi, I. A., Gibson, J. M., and Gilmour, I. 2006. Carbon and Nitrogen in Carbonaceous Chondrites: Elemental Abundances and Stable Isotopic Compositions. *Meteoritics & Planetary Science* 41: 1899–918.
- Rayleigh, L. 1942. The Stone-Iron Meteorites Called Pallasites: A Synthetic Study of Their Structure and Probable Mode of Formation. *Proceedings of the Royal Society of London A* 179: 386–93.
- Schmitt, W., Palme, H., and Wanke, H. 1989. Experimental Determination of Metal/Silicate Partition Coefficients for P, Co, Ni, Cu, Ga, Ge, Mo, and W and Some Implications for the Early Evolution of the Earth. *Geochimica et Cosmochimica Acta* 53: 173–85.
- Scott, E. R. D. 1977a. Pallasites—Metal Composition, Classification and Relationships with Iron Meteorites. *Geochimica et Cosmochimica Acta* 41: 349–60.
- Scott, E. R. D. 1977b. Formation of Olivine-Metal Textures in Pallasite Meteorites. *Geochimica et Cosmochimica Acta* 41: 693–710.
- Scott, E. R. D. 1977c. Geochemical Relationships Between Some Pallasites and Iron Meteorites. *Mineralogical Magazine* 41: 265–72.
- Scott, E. R. D. 2007. Impact Origins for Pallasites (Abstract #2284). 38th Lunar and Planetary Science Conference. CD-ROM.
- Scott, E. R. D., and Taylor, G. J. 1990. Origins of Pallasites at the Core–Mantle Boundaries of Asteroids (Abstract). 21st Lunar and Planetary Science Conference. p. 1119.
- Tarduno, J. A., Cottrell, R. D., Ferrière, L., and Scott, E. R. D. 2014. Preliminary Paleomagnetic Analysis of the Eagle Station Pallasite (Abstract #1945). 45th Lunar and Planetary Science Conference. CD-ROM.
- Tollari, N., Toplis, M. J., and Barnes, S.-J. 2006. Predicting Phosphate Saturation in Silicate Magmas: An Experimental Study of the Effects of Melt Composition and Temperature. *Geochimica et Cosmochimica Acta* 70: 1518–36.
- Ulf-Muller, F. 1998. Effects of Liquid Immiscibility on Trace Element Fractionation in Magmatic Iron Meteorites: A Case Study of Group IIIAB. *Meteoritics & Planetary Science* 33: 207–20.
- Warren, P. H. 2012. Parent Body Depth-Pressure-Temperature Relationships and the Style of the Ureilite Anatexis. *Meteoritics & Planetary Science* 47: 209–27.
- Wasson, J. T. 1999. Trapped Melt in IIIAB Irons: Solid/Liquid Elemental Partitioning during the Fractionation of the IIIAB Magma. *Geochimica et Cosmochimica Acta* 63: 2875–89.
- Wasson, J. T. 2017. Formation of Non-Magmatic Iron-Meteorite Group IIE. *Geochimica et Cosmochimica Acta* 53: 396–416.
- Wasson, J. T., and Choi, B.-G. 2003. Main-Group Pallasites: Chemical Composition, Relationship to IIIAB Irons, and Origin. *Geochimica et Cosmochimica Acta* 67: 3079–96.
- Wasson, J. T., Huber, H., and Malvin, D. J. 2007. Formation of IIAB Iron Meteorites. *Geochimica et Cosmochimica Acta* 71: 760–81.
- Wasson, J. T., and Kallemeyn, G. W. 1988. Composition of Chondrites. *Philosophical Transactions of the Royal Society of London A* 328: 535–44.
- Wasson, J. T., and Richardson, J. W. 2001. Fractionation Trends among IVA Iron Meteorites: Contrasts with IIIAB Trends. *Geochimica et Cosmochimica Acta* 65: 951–70.
- Yang, C. W., Williams, D. B., and Goldstein, J. I. 1996. A Revision of the Fe-Ni Phase Diagram at Low Temperature. *Journal of Phase Equilibria* 17: 522–31.
- Yang, J., Goldstein, J. I., and Scott, E. R. D. 2010. Main-Group Pallasites: Thermal History, Relationship to IIIAB Irons, and Origin. *Geochimica et Cosmochimica Acta* 74: 4471–92.

## SUPPORTING INFORMATION

Additional supporting information may be found in the online version of this article.

**Table S1.** Profiles of chemical composition (wt%) in 3  $\mu\text{m}$ , from the center to the edge of olivine grains in the Karavannoe pallasite.

**Table S2.** Profiles of chemical composition (wt%) in 2  $\mu\text{m}$ , from the center to the edge of olivine grains in the Karavannoe pallasite.